Low significance of foreshock activity in Southern California

L. Moutote[1], D. Marsan[2], O. Lengliné[1]and Z. Duputel[1]

[1]Institut de Physique du Globe de Strasbourg, UMR7516, Université de Strasbourg/EOST, CNRS, Strasbourg, France.

[2]Institut des Sciences de la Terre, UMR5275, Université Savoie Mont Blanc, CNRS, Le Bourget du Lac, France.

Pre-print Warning

Key Points:

- We reevaluate previous reports of significantly elevated seismic activity prior to large earthquakes in southern California
- Accounting for temporal clustering of earthquakes, we find that less than 10% mainshocks are preceded by anomalous foreshock sequences.
- The other sequences are explained by background seismicity, cascades of foreshocks or by recurrent fluctuations in seismicity rate.

Corresponding author: Luc Moutote, lmoutote@unistra.fr

Abstract

Earthquakes preceding large events are commonly referred as foreshocks. They are often considered as precursory signals reflecting the nucleation process of the main rupture. Such foreshock sequences may also be explained by cascades of triggered events. Recent advances in earthquake detection is a motivation to reevaluate seismicity variations prior to mainshocks. Based on a highly complete earthquake catalog, Trugman and Ross (2019) and van den Ende and Ampuero (2020) suggested that mainshocks in southern California are often preceded by anomalously elevated seismic activity. These studies assume a time-independent seismicity and thus neglect earthquake interactions. In this study, we test the same catalog against the Epidemic Type Aftershock Sequence model that accounts for earthquake clustering. We find that less than 5 out of 53 selected mainshocks (10%) are preceded by significantly elevated seismicity rates. This suggest that foreshock observations can generally be explained by background seismicity and by cascades of earthquakes even in highly complete earthquakes catalogs.

Plain Language Summary

Recent observations in southern California have suggested that the majority of large earthquakes are preceded by an elevated seismic activity. The anomalous character of those foreshock sequences is debated since elevated seismic activities are often not followed by a mainshock. Here we compare these observations to a seismicity model that accounts for the natural clustering of seismicity due to earthquake interactions. Even using a highly complete earthquake catalog, we find that the large majority of mainshocks are not preceded by an anomalous foreshock activity.

1 Introduction

Large earthquakes are often preceded by accelerating seismic activity (Jones & Molnar, 1976; Bouchon et al., 2013; Marsan et al., 2014). Although these foreshock sequences are often referred to as precursors, a somewhat ironical problem is the inherent difficulty to identify earthquakes as foreshocks before the mainshock occurs. In addition, we still do not fully understand the physical mechanisms that generate foreshocks and the reason why they occur. Two competing conceptual models have been proposed (Mignan, 2014). In the first model, foreshock stress changes contribute to a slow cascade of random failures (possibly mediated by aseismic afterslip) ultimately leading to the mainshock (Helmstetter & Sornette, 2003; Marzocchi & Zhuang, 2011; Ellsworth & Bulut, 2018). The second model proposes that foreshocks are tracers of an evolving nucleation process preceding the mainshock rupture (Dodge et al., 1996; Bouchon et al., 2011; Kato et al., 2016). The aseismic vs seismic contributions to the overall moment release during the precursory phase is ultimately what distinguishes these two models. Unfortunately, the aseismic part is generally difficult or merely impossible to estimate from the available observations, and one therefore needs to resort to indirect arguments, often pertaining to the spatial and temporal distribution of the foreshocks. Although recent observations of slow deformation lasting days to months before the mainshock favor the triggering of foreshocks by aseismic preslip (Socquet et al., 2017; Mavrommatis et al., 2014; Ito et al., 2013), the aseismic character of such precursory motion is vigorously debated (Ruiz et al., 2014; Bedford et al., 2015). In addition, foreshock sequences are not observed systematically before large earthquakes. However, this lack of systematic precursory observations might partly be due to the incompleteness of current seismicity catalogs (Mignan, 2014; Ross et al., 2019)

The southern California catalog was recently enhanced thanks to the template matching analysis conducted by Ross et al. (2019). The resulting QTM (Quake Template Matching) catalog includes more than 850,000 earthquakes (for the higher choice of threshold, see Section 2.1) in a 10 year-long period from 2008 to 2017 and can be complete for magnitudes near or below zero for the best resolved regions. Such a high degree of completeness of the QTM catalog motivates the evaluation of the statistical significance of seismic activity preceding large earthquakes in southern California. By comparing seismic activity before $M \geq 4$ earthquakes to a constant background rate, Trugman and Ross (2019, T&R from here on) estimated that 72% of mainshocks in the QTM catalog are preceded by an anomalously high seismic activity. The reported results suggest that detailed foreshock detection could bear important information about an impending earthquake. This interpretation was later questioned by van den Ende and Ampuero (2020, V&A from here on) which pointed out that T&R did not evaluate the significance of elevated foreshock activity compared to natural fluctuations in the seismicity rate. To assess the statistical significance of foreshock sequences, V&A compared foreshock activity with a model where earthquake inter-event times (IETs) are sampled independently from a gamma distribution. This approach is motivated by the fact that IETs in seismic catalog tends to follow a gamma, rather than an exponential distribution as assumed by T&R. Based on this analysis, V&A estimated that only 30% of mainshocks are preceded by anomalous foreshock activity, coming down to 18% when accounting for temporal fluctuations in background seismicity.

Although V&A improves previous estimates by T&R, their reanalysis still ignores the temporal clustering of seismicity. The random sampling approach of V&A assumes independent IETs, which is an over-simplification. Indeed, this approach is unable to explain local aftershock sequences prior to the mainshock, in which IETs are correlated rather than independent. In ”normal” earthquake sequences, the triggering of aftershocks leads to clusters of events during which the likelihood of triggering a mainshock is higher than at quiet times. Neglecting the temporal clustering of earthquakes is therefore a strong hypothesis that inherently recuses cascades of triggered seismicity as a possible explanation of foreshock sequences.

Going forward, we here assess more robustly what is the statistical significance of foreshock sequences accounting for the temporal clustering of earthquakes. In this work, we use the temporal Epidemic Type Aftershock Sequences (ETAS) model, in which the seismicity rate at each time is represented by the superposition of a background rate and a rate linked to the triggering from past events (Ogata, 1988). This model is the simplest that can reproduce both the gamma distribution of IETs (Saichev & Sornette, 2007) and the correlation of successive IETs. After selecting mainshocks using criteria similar to T&R and V&A, we extract ETAS parameters from the QTM catalog in the vicinity of each mainshock. We then compare the foreshock activity with ETAS predictions accounting for past seismicity. We find that the number of anomalous foreshock sequences is significantly reduced when accounting for temporal clustering (about 18% compared to 33% and 72% respectively in V&A and T&R). Focusing only on seismicity time-series that are best constrained, we estimate that less than 10% of mainshocks are preceded by significantly anomalous foreshock activity.

2 Data and methods

2.1 Mainshock selection

We noticed that the full QTM catalog used by T&R and V&A suffers from episodic bursts of false detections, that occur due to a too low detection threshold (threshold fixed at 9.5 times the median absolute deviation (MAD) of the stacked correlation function) . These bursts are easy to identify as they start or end at midnight, which is due to the MAD computation performed over 24 hour long period starting at 00h00 UTC. To avoid any contamination of our analysis by such artifacts, we instead use the higher quality QTM catalog with a detection threshold at 12 times the MAD, for which these transients vanish or are strongly attenuated. In order to provide a fair comparison with previous results, we also present our analysis performed on the full catalog in the supporting information (Text S3 and Figure S4 and S5).

Using the higher quality QTM catalog, we then select 53 mainshocks with criteria resembling those of T&R. A mainshock must have magnitude $M \geq 4$, and must occur from 2009/01/01 to 2016/12/31 within the geographic coordinates ranges [32.68°N, 36.2°N] and [118.80°W, 115.4°W]. To be selected, a mainshock must be preceded by at least 10 earthquakes with no larger magnitude event in the year before and within a 20×20 km horizontal box around its epicenter. For each selected mainshock, we extract a 10-year long local catalog that includes all the seismicity observed within the 20×20 km box with no depth cutoff.

For each local catalog, we evaluate the local magnitude of completeness M_c and remove all events with a magnitude $M < M_c$. The local M_c is estimated manually as the maximum of the local Gutenberg-Richter frequency-magnitude distribution. Figure S1 of the supporting information shows the 53 local Gutenberg-Richter frequency-magnitude distributions and the corresponding estimated M_c.

2.2 V&A approach with synthetic ETAS catalogs

In this section, we illustrate the limitations of V&A approach by applying it to synthetic realizations of a temporal ETAS seismicity model (cf., Figure 1). The ETAS model has two main ingredients: first, a background term which is time-independent and follows a Poisson process; second, a triggered term which depends on the past earthquake activity. The conditional intensity of the ETAS model (Ogata, 1988;

Zhuang et al., 2012) is :

$$\lambda(t) = \mu + \sum_{i|t_i<t} A\mathrm{e}^{\alpha(M_i - M_c)}(t - t_i + c)^{-p} \tag{1}$$

where μ is the time-independent background seismicity rate. The sum in the right hand side of equation (1) describes the expected aftershock seismicity rate at time t triggered by all previous events. A and α are constant parameters describing respectively the global aftershock productivity of the region and the magnitude dependence in the number of triggered events. M_c is the magnitude of completeness whereas c and p are the parameters of the Omori-Utsu law describing the time-decay in the aftershock seismicity rate.

Synthetic ETAS catalogs are able to reproduce temporally clustered seismicity. In such model, clustering activity emerges spontaneously from random cascades of aftershocks. This is illustrated in Figure 1a with observable aftershock sequences initially triggered by several $M \sim 3$ events and a $M = 4$ earthquake. By construction, such a synthetic catalog does not contain any foreshock activity other than that due to earthquake interactions. As for natural seismicity, the distribution of inter-event times (IETs) of an ETAS catalog tends to a gamma distribution (cf., Figure 1b). Following V&A, if we independently resample the IETs of Figure 1b , we obtain for instance the catalog shown in Figure 1c in which the temporal clustering disappeared (even if IETs have the same distribution by construction). In particular, there is no visible aftershock sequences following $M \sim 3$ events contrary to catalog observations. To further quantify the limitations of such a random sampling approach, we generate 1000 realizations of 5-years duration synthetic ETAS catalogs and extract $M \geq 4$ mainshocks as in section 2.1. Following V&A, we then sample a Probability Mass Function (PMF) of the expect number of event in 20 day windows assuming independent gamma realization of IETs (Figure 1d). We extract the probability p that independent IETs can explain foreshock activity by confronting this PMF with the "observed" number of events in the 20 days prior synthetic mainshocks (Figure 1e). Assuming the same significance threshold of $p < 0.01$ as in T&R and V&A, Figure 1e shows that more than 10% of mainshocks are preceded by an anomalous seismic activity even though they are actually explained by cascades of aftershocks. The 1000 synthetic ETAS catalogs are also tested against the second approach of V&A. In this approach, the PMF is sampled empirically by counting the number of events in 20-days windows randomly distributed over the $[-380, -20[$ period with respect to the mainshock origin time (Figure1d). As for independent IETs sampled from a gamma distribution, the empirical approach of V&A shows that more than 10% of mainshocks are preceded by an anomalous earthquake activity (Figure1f). Therefore, the two approaches of V&A struggle to properly consider causal earthquakes interactions and their corresponding seismicity rate increases.

2.3 Inversion of ETAS parameters

In this study, we test, as a null-hypothesis, that seismicity rates observed prior to each mainshock behave according to an ETAS model. Anomalous precursory seismicity is then defined as a time period immediately prior to the mainshock with a significantly higher earthquake rate compared to the expected rate predicted by the ETAS model.

For local catalogs associated with each mainshock, we fit the temporal ETAS model by maximizing a likelihood function with an Expectation - Maximization (EM) algorithm (Veen & Schoenberg, 2008). We estimate parameters A, c, p, α and μ in equation (1) (all parameter values can be found in the supporting information). We run a first inversion where the ETAS parameters are constrained to be positive. We note that most α values are close to one. Larger α values are actually expected according to window-based methods (Helmstetter, 2005; Felzer et al., 2004), as well as following the

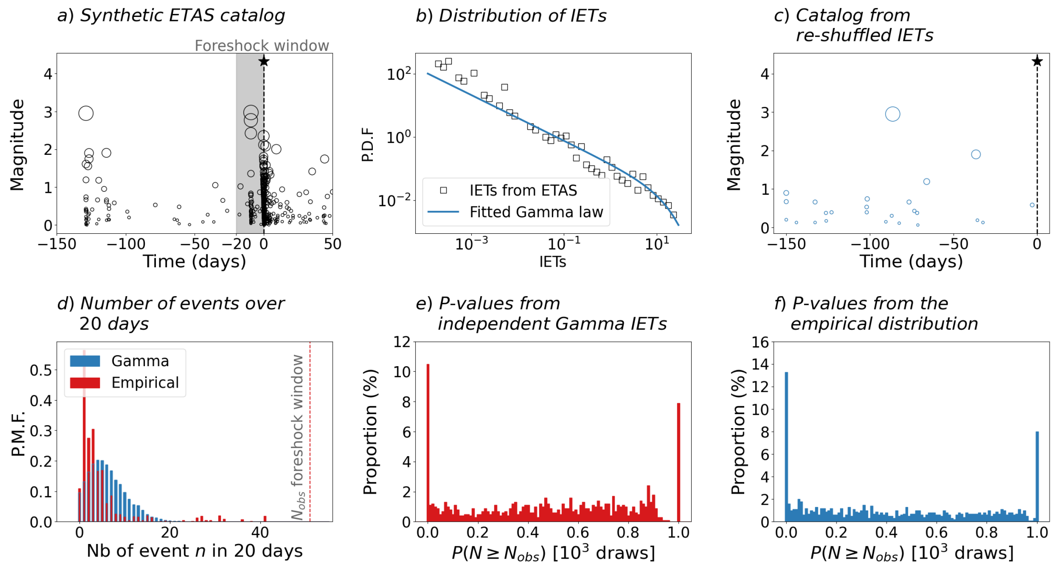

Figure 1. **(a)** A realisation of a synthetic ETAS catalogue (α=2, p=1.1, c=10^{-3}, μ=0.1, β=2.23 corresponding to a b-value of 1 for the Gutenberg-Richter law, M_c=0) and its 20-day foreshock window as defined by van den Ende and Ampuero (2020). The $M \geq 4$ is considered here as the mainshock. **(b)** IETs distribution of this ETAS catalogue observed in the $[-380, -20[$ window and its fitted gamma law. **(c)** IETs reshuffling of the $[-380, -20[$ days window. Note that clustered events are no longer related to the distribution of magnitude. **(d)** The sampled gamma/empirical probability mass functions (PMFs) of the number of events expected in the 20-day window according to the two approaches of V&A. The red vertical dashed line corresponds to the number of events N_{obs} actually observed in the ETAS 20-day foreshock window. **(e)** Distribution of the foreshock probability $p = P(N \geq N_{obs})$ using V&A first approach (drawing of independent, gamma-distributed IETs), for the 1000 synthetic ETAS catalogs. **(f)** Same as (e) but for the V&A second (empirical) approach (counting the number of earthquakes within random 20 day windows included in the $[-380, -20[$ period before the mainshock). More than 10% of the ETAS foreshock windows are detected with an anomalous seismicity ($p < 0.01$) although no anomaly is actually present. In (e) and (f), the p-value spike at 1 correspond to windows with $N_{obs} = 0$ or N_{obs} far from the minimum of the gamma/empirical PMF

argument that Bath's law, i.e., the fact that the difference in magnitude between the mainshock and its largest aftershock is independent of the mainshock's magnitude, requires that $\alpha = \beta = b \ln 10$ (Davidsen and Baiesi (2016) and references therein). Moreover, it has been shown that α estimates are particularly prone to model errors (e.g., Hainzl et al. (2008, 2013)) and censoring effects (Sornette and Werner (2005); Seif et al. (2017)). Nandan et al. (2017) found that the α value is expected to vary between 1.7 and 2.2 when considering a larger portion of California and a longer period than the QTM catalog. A α value close to 2 may thus represent a more realistic value of the aftershock productivity for Californian earthquakes. Therefore, we perform a second inversion where we impose that $\alpha = 2$. We thus obtain two sets of ETAS parameters (referred to as "α free" and "$\alpha = 2$" sets) to model the seismicity of local catalogs around each mainshock.

2.4 Detection of seismicity anomalies based on the ETAS model

We test the hypothesis H_0 that the observed number of events in a time window T is smaller or equal than the number of events predicted by the ETAS model for both of the parameter estimates. If H_0 is rejected, an anomalous earthquake sequence is detected in T, suggesting that a mechanism other than simple cascading is required to explain such a high seismicity rate. The conditional intensity function in equation (1) allows to directly compute an expected seismicity rate at any time t from the set of ETAS parameters (A, c, p, α and μ) and the knowledge of past seismicity ($t_i < t, M_i$). By integrating this modelled seismicity rate, we can compute the expected number of earthquakes $\overline{N}$ in a time interval T:

$$\overline{N}(t,T) = \int_{t-T}^{t} \lambda(u)\,\mathrm{d}u \tag{2}$$

Here we set $T = 20$ days similar to T&R, which choice was also adopted by V&A. We compute $\overline{N}$ over 20-day sliding windows, with a 1 day shift between two consecutive windows, and covering the full time range of the QTM catalog (i.e., 10 years). For local catalogs around each mainshock, we then obtain two time-series of $\overline{N}$ generated using the two sets of inverted ETAS parameters (α free and $\alpha = 2$). Knowing $\overline{N}$, the probability of actually observing N_{obs} earthquakes in a given 20-day time-interval is given by the Poisson distribution with mean $\overline{N}$:

$$P(N_{obs}) = \frac{\overline{N}^{N_{obs}}\mathrm{e}^{-\overline{N}}}{N_{obs}!} \tag{3}$$

We then define the probability of observing at least N_{obs} events over 20 days for the null hypothesis as:

$$p = P(N \geq N_{obs}) = 1 - \sum_{n=0}^{N_{obs}-1} \frac{\overline{N}^{n}\mathrm{e}^{-\overline{N}}}{n!} \tag{4}$$

Following T&R and V&A, we use the probability threshold $p < 0.01$ to reject the hypothesis H_0 that N_{obs} is in agreement with the expected number of events $\overline{N}$. A small p-value would therefore correspond to anomalously elevated seismicity rate compared with ETAS predictions.

3 Results

The detection of seismicity rate anomalies in a 20-days sliding window is illustrated in Figure 2 for the seismicity located in the vicinity of 4 mainshocks. For each mainshock, the top subplot shows the time-evolution of p-values measured for the two set of ETAS parameters (α free and $\alpha = 2$) while the bottom subplot shows the observed seismicity (i.e., magnitude vs time). For the two examples on top (Mainshock IDs 10832573 and 37301704), we notice that the foreshock activity is consistent with ETAS predictions with a p-value above 0.01 in the 20-days window prior to the mainshock. In these cases, our null hypothesis H_0 is verified for both ETAS parameter estimates and there is no clear evidence of an elevated foreshock activity. The two examples on the bottom (Mainshock IDs 14898996 and 37299263) show p-values that are below 0.01 before the mainshock for both sets of ETAS parameters. In these cases, the observed foreshock seismicity is not consistent with a cascading hypothesis.

In total, we find that 10 out of 53 mainshocks are preceded by an anomalous foreshock activity with respect to ETAS predictions. However, this result must be taken in perspective with the overall ability of our ETAS models to explain fluctuations in seismicity rates over the entire catalog. As pointed out by V&A, the significance of an anomalous foreshock activity is reduced if seismicity anomalies are frequently

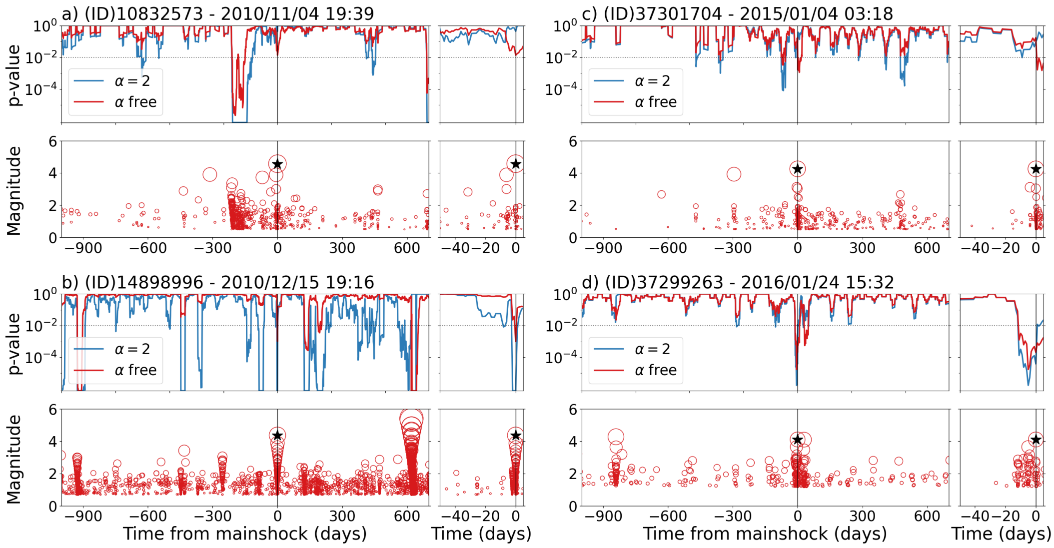

Figure 2. The 20-day sliding window analysis for 4 examples of mainshocks (black star at t=0) and their local catalog. Mainshocks QTM IDs are (a) 10832573, (b) 37301704, (c) 14898996 and (d) 37299263. (Top graphs) probability p that ETAS explain the observed seismicity, computed for for the two set of ETAS parameters α=2 and α free. The significance threshold of p=0.01 is shown with the horizontal dotted line. (Bottom graphs) magnitude vs time for the local catalogs in the 20×20 km box around each mainshock. The right inset is a zoom around the foreshock window.

detected without being followed by a large event. The significance of an anomalous foreshock sequence should thus be assessed given the overall ability of ETAS predictions to explain the seismicity in the vicinity of the mainshock. For example, in the case of mainshock ID 14898996 in Figure 2c, ETAS predictions are unable to explain the observed seismicity several times over the duration of the catalog. Our null hypothesis H_0 is thus rejected at numerous occasions with p-values smaller than the foreshock window before and after the mainshock origin time. This behaviour strongly affects the significance of the foreshock window result. On the other hand, Figure 2d shows that mainshock 37299263 presents an anomalous seismicity rate almost exclusively in the 20 days preceding the mainshock. Such an elevated seismicity rate is thus highly correlated with the mainshock occurrence.

Therefore, to quantify the statistical significance of detected foreshock anomalies, we compare p-values in the foreshock window with the distribution of p-values over the entire 10-year catalog. For each mainshock, an anomalous foreshock activity is considered significant if $\hat{p}$, the proportion of 10-year p-values lower or equal than the foreshock p-value, is less than 1%. This threshold of 1% allows to discriminate catalogs with frequent anomalous activities to focus on foreshock sequences that corresponds to the strongest anomalies of their region. This is summarized in Figure S3 and Text S1 of the supporting information. Using such temporal significance criteria, we identify that 5 out of the 10 anomalous sequences already mentioned occur in regions with recurrent seismicity anomalies stronger than the foreshock one. Therefore, we argue that only 5 out of 53 mainshocks (∼10%) are preceded by statistically significant elevated foreshock activity according to our null hypothesis.

We complement this analysis by declustering the local catalogs. The probability ω_i that earthquake i is a background earthquake is defined as $\omega_i = \frac{\mu}{\lambda(t_i)}$, and can be calculated once the ETAS parameters are estimated. We then simply count the numbers of background earthquakes as the sums of ω_i in 20 day long windows. We denote N_0 this count for the last 20 days prior to the mainshock, and by N all the counts for all the time windows before the mainshock (not just the last one). Following the same rationale that stimulated our previous analysis, we first compare N_0 to the Poisson distribution with a mean $\bar{N}$ equal to the mean of N, select the mainshocks for which $P(> N_0|\bar{N}) < 0.01$ for the two sets of ETAS parameters (1st test), and finally check whether these selected sequences display other anomalously strong bursts of background earthquakes by computing the probability that N can be greater than N_0 (2nd test). We finally select those short-listed mainshocks for which the latter probability is less than 0.01 (again, for the two sets of ETAS parameters). Figure 3 shows the results of this declustering approach. Only mainshocks 14598228 and 14600292 effectively pass the two tests, and are thus seen as preceded by anomalous foreshock sequences according to this declustering approach. These two anomalous sequences were also identified in our previous approach based on the predicted number of events according to the ETAS model.

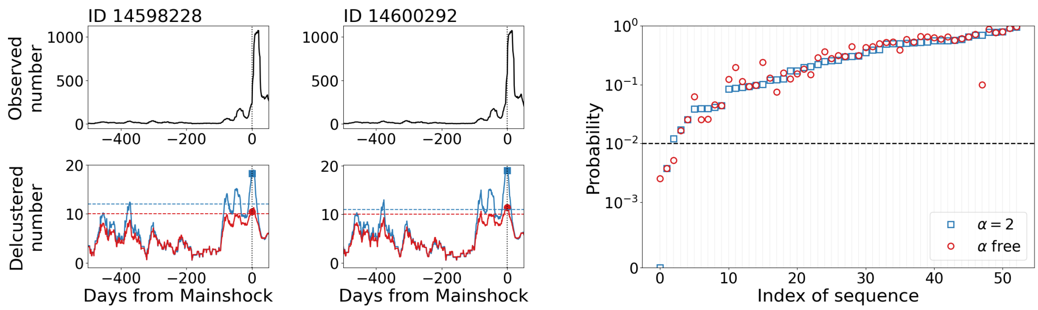

Figure 3. Number of earthquakes in 20 day long windows counting (top) all earthquakes and (bottom) background earthquakes only, for the two mainshocks that are identified as having an anomalous foreshock sequence according to the declustering analysis. The number for the last window prior to the mainshock is shown with a thick square. The dashed lines show, for the two sets of ETAS parameters (α free in red, $\alpha = 2$ in blue) the limit over which the Poisson probability becomes less than 0.01. Right: probability $P(N{>}N_0)$ that the last 20 days are anomalously active compared to the past, for the two sets of ETAS parameters; the sequence is selected as anomalous after declustering if this probability is less than 0.01 (2nd test) and if N_0 is above the dashed line (1st test). Mainshocks 14598228 and 14600292 correspond to indices 0 and 1 on this graph, and are the only mainshocks with both probabilities less than 0.01. All indices can be linked with their mainshock ID thanks to Table S2.

4 Discussion

We use the highly complete QTM catalog of Ross et al. (2019) to reassess the significance of anomalous foreshock activity previously reported in southern California by T&R and V&A. As mentioned before, those studies do not account for the temporal clustering of earthquakes, although this clustering is considered as one of the possible origin to accelerating seismic activity observed before large earthquakes. In practice, small $M < 4$ earthquakes trigger small aftershock sequences during which a larger $M > 4$ event is more likely to occur than at more quiet times. Thus, high activity preceding a mainshock can naturally stem from earthquake clustering without necessarily requiring an external pre-slip phenomena.

We first assess the probability p that a given foreshock sequence can be explained by "normal" earthquake clustering. Using $p < 0.01$ as a threshold, our results indicate that $\sim 18\%$ (10 out of 53) of mainshocks are preceded by anomalous earthquake sequences (compared to 33% and 72% respectively in V&A and T&R). When accounting for other increases in seismicity rates not related to a mainshock, only $\sim 10\%$ of mainshocks (5 out of 53) are immediately preceded by a foreshock-specific anomalous seismicity rate that cannot be explained by background seismicity or cascades of foreshocks. The complementary declustering approach further restricts the statistically significant foreshock activity to only two sequences. A possible over-estimation of the background rate can be a cause for this more conservative selection. Anomalous mainshock IDs detected in T&R, V&A and this study can be found in Table S1 of the supporting information. The Southern Californian location of these sequences are also compared in Figure S7. The 20-days evolution of the 5 anomalous foreshock sequences detected in the first approach of this study are presented in details in Text S2 and Figure S6.

We must emphasize that these results, along with those of T&R and V&A, likely depends on the initial choice of focusing on foreshocks in a 20 days period prior to each mainshock. Using a longer or shorter time-window may therefore provide different results. Moreover, the fixed 20×20 km horizontal spatial window used in this study implies that all events in this box are evaluated with the same weight. This can artificially enhance the triggering role of foreshocks that are relatively far from the mainshock. The ETAS model used here would need to be extended to a space-time model in order to exploit the distance between earthquakes and to help to discriminate such cases (Zhuang et al., 2011, for a review).

Furthermore, the exact number of detected foreshock anomalies obviously depends on the significance threshold that we have fixed to $p < 0.01$ following T&R and V&A. To assess the impact of this arbitrary choice, we evaluate how the proportion of detected anomalous foreshock sequences changes as a function of the p-value threshold p_{thresh}. This result is compared with the proportion of windows that have $p < p_{thresh}$ without being followed by a mainshock (i.e., false positives). We thus compute the Receiver Operating Characteristic (ROC) curve as shown in Figure 4. If the occurrence of anomalously elevated activity was not a sign of an incoming mainshock, then the ROC curve would follow a 1 to 1 straight line (hereafter referred to as the no-gain line). We find that there is positive correlation between preceding high activity and mainshock occurrence: the information gain is measured by the ratio of true positives over false positives, which is practically constant and close to 6 for $p_{thresh} \leq 0.05$. We however notice that significant departure from this no-gain line also exists in ETAS simulations computed with the same 53 sets of parameters as obtained for the local catalogs. Figure 4 shows that a large p_{thresh} (i.e., > 0.01) allows to detect anomalous foreshock activities (i.e., a positive gain) in ETAS simulations, even though there is by definition no pre-slip in this model. This is caused by the clustering properties of the model: in the rare occasions where the observed number of earthquakes N_{obs} in a window largely exceeds the expected number $\overline{N}$, then the occurrence of earthquakes immediately after this window is more likely, including the occurrence of a mainshock. As an effect, the ROC curve departs from the no-gain line. We however notice that there is no information gain on the magnitude of the forthcoming earthquakes, as expected. We conclude that choosing a large value of p_{thresh} may lead to the detection of "foreshock cascades" prior to mainshocks, which are not related to aseismic processes (e.g., preslip). According to our simulations, $p_{thresh} = 0.01$ appears as an acceptable threshold to discriminate a cascading behaviour from other possible processes: the information gain for ETAS is about 2, compared to about 6 for the observed seismicity (cf., $p_{thresh} = 0.01$ in Figure 4). This additional gain is mostly controlled by the 10 sequences we found to be anomalous: quite obviously, removing them from the calculations implies that the ROC curve is equal to zero at $p_{thresh} = 0.01$.

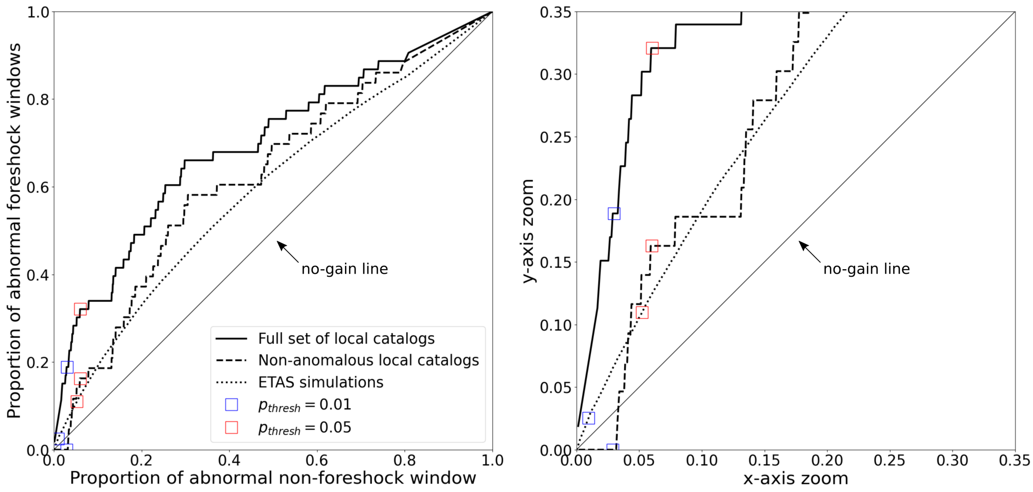

Figure 4. Receiver Operating Characteristic (ROC) curves for our detection of anomalous foreshock windows. For a varying threshold p-value p_{thresh}, curves show the proportion of foreshock windows below p_{thresh} against the proportion of non-foreshock windows below p_{thresh}. ROC curves are drawn for the full set of 53 local catalogs and after removing the 10 anomalous sequences of section 3 (with $p < 0.01$). We also include the ROC curve corresponding to the average of 53 sets of 1000 ETAS simulations computed using the α free ETAS parameters obtained in section 2.3. Note that ETAS simulations display a curved ROC, the departure from the "no-gain" line being particularly clear when considering large p_{thresh} values. This departure is weak for $p_{thresh} \leq 0.01$, with a gain of about 2 at maximum ($p_{thresh} = 0.01$).

5 Conclusions

According to our analyses, the low magnitude of completeness of the QTM catalog does not warrant the detection of aseismically-driven foreshock sequences in the 20-days window preceding mainshock events. More than 90% of observed foreshock sequences are indeed well explained by a simple cascading model even when the magnitude of completeness is as low as $M_c = 0$.

High quality earthquake datasets complete to low magnitudes are in any case required to pursue and develop efforts for understanding when and where aseismic pre-slip can lead to a large shock. First, increasing the location accuracy and the number of small earthquakes substantially improves the statistical significance of any test conducted to assess the reality of pre-slip processes, when comparing to the cascade (null) hypothesis. Second, the availability of large datasets allows to increase the number of potential mainshocks to be analyzed, hence offering more robust conclusions. Finally, we suggest that pre-slip seismicity analysis should be evaluated along other near-fault observables (such as GPS or tiltmeter data) to independently assess any possible aseismic mechanisms at work during the preparation of large earthquakes.

Acknowledgments

This study is based on the QTM seismicity catalog accessible via the Southern California Earthquake Data Center (https://scedc.caltech.edu). This project has received funding from the European Research Council (ERC, under the European Union's Horizon 2020 research and innovation program under grant agreement No. 805256).

References

Bedford, J., Moreno, M., Schurr, B., Bartsch, M., & Oncken, O. (2015). Investigating the final seismic swarm before the Iquique-Pisagua 2014 Mw 8.1 by comparison of continuous gps and seismic foreshock data. *Geophysical Research Letters*, *42*(10), 3820–3828.

Bouchon, M., Durand, V., Marsan, D., Karabulut, H., & Schmittbuhl, J. (2013). The long precursory phase of most large interplate earthquakes. *Nature Geoscience*, *6*(4), 299–302. doi: 10.1038/ngeo1770

Bouchon, M., Karabulut, H., Aktar, M., Ozalaybey, S., Schmittbuhl, J., & Bouin, M.-P. (2011). Extended nucleation of the 1999 Mw 7.6 Izmit earthquake. *Science*, *331*(6019), 877–880. doi: 10.1126/science.1197341

Davidsen, J., & Baiesi, M. (2016). Self-similar aftershock rates. *Physical Review E*, *94*(2), 022314. doi: 10.1103/PhysRevE.94.022314

Dodge, D. A., Beroza, G. C., & Ellsworth, W. L. (1996). Detailed observations of California foreshock sequences: Implications for the earthquake initiation process. *Journal of Geophysical Research: Solid Earth*, *101*(B10), 22371–22392.

Ellsworth, W. L., & Bulut, F. (2018). Nucleation of the 1999 Izmit earthquake by a triggered cascade of foreshocks. *Nature Geoscience*, *11*(7), 531–535. doi: 10.1038/s41561-018-0145-1

Felzer, K. R., Abercrombie, R. E., & Ekström, G. (2004). A common origin for aftershocks, foreshocks, and multiplets. *Bulletin of the Seismological Society of America*, *94*(1), 88–98. doi: 10.1785/0120030069

Hainzl, S., Christophersen, A., & Enescu, B. (2008). Impact of earthquake rupture extensions on parameter estimations of point-process models. *Bulletin of the Seismological Society of America*, *98*(4), 2066–2072. doi: 10.1785/0120070256

Hainzl, S., Zakharova, O., & Marsan, D. (2013). Impact of aseismic transients on the estimation of aftershock productivity parameters. *Bulletin of the Seismological Society of America*, *103*(3), 1723–1732. doi: 10.1785/0120120247

Helmstetter, A. (2005). Importance of small earthquakes for stress transfers and earthquake triggering. *Journal of Geophysical Research*, *110*(B5), B05S08. doi: 10.1029/2004JB003286

Helmstetter, A., & Sornette, D. (2003). Foreshocks explained by cascades of triggered seismicity. *Journal of Geophysical Research*, *108*(B10). doi: 10.1029/2003JB002409

Ito, Y., Hino, R., Kido, M., Fujimoto, H., Osada, Y., Inazu, D., … Ashi, J. (2013). Episodic slow slip events in the Japan subduction zone before the 2011 Tohoku-Oki earthquake. *Tectonophysics*, *600*, 14–26.

Jones, L., & Molnar, P. (1976). Frequency of foreshocks. *Nature*, *262*(5570), 677–679.

Kato, A., Fukuda, J., Kumazawa, T., & Nakagawa, S. (2016). Accelerated nucleation of the 2014 Iquique, Chile Mw 8.2 earthquake. *Scientific Reports*, *6*(1), 24792. doi: 10.1038/srep24792

Marsan, D., Helmstetter, A., Bouchon, M., & Dublanchet, P. (2014). Foreshock activity related to enhanced aftershock production. *Geophysical Research Letters*, *41*(19), 6652–6658.

Marzocchi, W., & Zhuang, J. (2011). Statistics between mainshocks and foreshocks in Italy and Southern California. *Geophysical Research Letters*, *38*(9).

Mavrommatis, A. P., Segall, P., & Johnson, K. M. (2014). A decadal-scale deformation transient prior to the 2011 Mw 9.0 Tohoku-oki earthquake. *Geophysical Research Letters*, *41*(13), 4486–4494. doi: 10.1002/2014GL060139

Mignan, A. (2014). The debate on the prognostic value of earthquake foreshocks: A meta-analysis. *Scientific Reports*, *4*(1), 4099.
Nandan, S., Ouillon, G., Wiemer, S., & Sornette, D. (2017). Objective estimation of spatially variable parameters of epidemic type aftershock sequence model: Application to California. *Journal of Geophysical Research: Solid Earth*, *122*(7), 5118–5143. doi: 10.1002/2016JB013266
Ogata, Y. (1988). Statistical models for earthquake occurrences and residual analysis for point processes. *Journal of the American Statistical Association*, *83*(401), 9–27. doi: 10.1080/01621459.1988.10478560
Ross, Z. E., Trugman, D. T., Hauksson, E., & Shearer, P. M. (2019). Searching for hidden earthquakes in Southern California. *Science*, *364*(6442), 767–771. doi: 10.1126/science.aaw6888
Ruiz, S., Metois, M., Fuenzalida, A., Ruiz, J., Leyton, F., Grandin, R., ... Campos, J. (2014). Intense foreshocks and a slow slip event preceded the 2014 Iquique Mw 8.1 earthquake. *Science*, *345*(6201), 1165–1169.
Saichev, A., & Sornette, D. (2007). Theory of earthquake recurrence times. *Journal of Geophysical Research*, *112*(B4). doi: 10.1029/2006JB004536
Seif, S., Mignan, A., Zechar, J. D., Werner, M. J., & Wiemer, S. (2017). Estimating ETAS: The effects of truncation, missing data, and model assumptions. *Journal of Geophysical Research: Solid Earth*, *122*(1), 449–469. doi: 10.1002/2016JB012809
Socquet, A., Valdes, J. P., Jara, J., Cotton, F., Walpersdorf, A., Cotte, N., ... Norabuena, E. (2017). An 8 month slow slip event triggers progressive nucleation of the 2014 Chile megathrust. *Geophysical Research Letters*, *44*(9), 4046–4053. doi: 10.1002/2017GL073023
Sornette, D., & Werner, M. J. (2005). Apparent clustering and apparent background earthquakes biased by undetected seismicity. *Journal of Geophysical Research*, *110*(B9). doi: 10.1029/2005JB003621
Trugman, D. T., & Ross, Z. E. (2019). Pervasive foreshock activity across Southern California. *Geophysical Research Letters*, *46*(15), 8772–8781. doi: 10.1029/2019GL083725
van den Ende, M. P. A., & Ampuero, J. (2020). On the statistical significance of foreshock sequences in Southern California. *Geophysical Research Letters*, *47*(3). doi: 10.1029/2019GL086224
Veen, A., & Schoenberg, F. P. (2008). Estimation of space–time branching process models in seismology using an EM–type algorithm. *Journal of the American Statistical Association*, *103*(482), 614–624. doi: 10.1198/016214508000000148
Zhuang, J., Harte, D., Werner, M. J., Hainzl, S., & Zhou, S. (2012). Basic models of seismicity: Temporal models. *Community Online Resource for Statistical Seismicity Analysis*, *Theme V*(1).
Zhuang, J., Werner, M. J., Hainzl, S., Harte, D., & Zhou, S. (2011). Basic models of seismicity: Spatiotemporal models. *Community Online Resource for Statistical Seismicity Analysis*, *Theme V*(1), 20.